Heavy Ion Energy Deposition and SEE Intercomparison Within the RADNEXT Irradiation Facility Network

Rubén García Alía, *Member, IEEE*, Andrea Coronetti, *Member, IEEE*, Kacper Bilko, Matteo Cecchetto, Gerd Datzmann, Salvatore Fiore, *Member, IEEE*, and Sylvain Girard, *Senior Member, IEEE*

***Abstract*— RADNEXT is an EU-funded network of irradiation facilities and radiation effects' experts aimed at increasing the quantity and quality of user access to accelerator infrastructure and improving the diversity and harmonization across facilities. Along with beam provision to worldwide radiation effects' users, RADNEXT has an ambitious research program oriented at improving radiation effects' testing, of which an example of a heavy ion facility intercomparison at very different energy regimes is included in this work. In particular, energy deposition distributions in a silicon solid-state detector and the single-event upset (SEU) and multiple-cell upset (MCU) behavior are compared among heavy ion beams of similar LET, but very different energies (i.e., from the more classical ∼10 MeV/u regime up to several hundreds of MeV/u).**

***Index Terms*— Dosimetry, facilities, high-energy ions, single-event effects, solid-state detector, SRAM.**

I. Introduction and Motivation

THE EU-funded RADNEXT (RADiation facility Network for the EXploration of effects for indusTry and research, Grant Agreement ID: 101008126) project aims to create a network of facilities and related irradiation services, methodologies, and expertise for responding to the emerging needs of electronics components and system irradiation [1]. The four-year, 5-MEUR EU-funded project (which started on 1 June 2021 and is due to end 31 May 2025) is coordinated by the European Organization for Nuclear Research (CERN) and, as further detailed in Appendix A, includes a total of 30 other beneficiaries (i.e., recipients of EU funding) and nine associated partners. RADNEXT is part of the "Excellent Science—Research Infrastructures" Horizon 2020 main program and the "INFRAIA-02-2020—Integrating Activities for Starting Communities" topic.

The main objective of RADNEXT is that of bridging the gap between large scientific infrastructures (e.g., accelerators, reactors) and irradiation testing users. This is achieved, first, through the EU funding of user irradiation activities and related networking and research, but also by decreasing irradiation lead times, enhancing the irradiation service quality, and increasing the degree of harmonization across facilities and related to irradiation methodologies. To this end, more than 6000 h of EU-funded irradiation beam time will be made available to the worldwide radiation effects' community, through a beam proposal process that includes the evaluation by a user selection panel (USP) of international experts, which will be detailed later on in this article.

The RADNEXT project is mainly motivated by service-oriented needs and objectives, outlined in Appendix B, as well as by scientific and technical challenges and goals, described below.

RADNEXT has been conceived as a facility network capable of satisfying a very broad range of irradiation needs, including notably space, high-reliability atmospheric, high-energy accelerators (both scientific and medical), and fusion applications. Therefore, the network is built to cover a vast irradiation phase space, particularly in terms of particle species, particle energy, and linear energy transfer (LET), as well as beam intensity/flux and beam (or radiation field) size and penetration capacity.

The radiation environments and applications that RADNEXT targets are summarized in Table I, along with key single-event effects (SEEs) testing requirements, mostly in qualitative terms, but also including quantitative values, mainly for orientation purposes.

In this article, the focus is set on SEE testing as the main driver for accelerator-based irradiation testing; however, total non-ionizing dose (TNID) effects, also requiring testing in accelerator or reactor facilities, are part of the RADNEXT transnational access (TA) beam provision, whereas total ionizing dose (TID) effects, typically assessed experimentally through radioactive sources (e.g., cobalt-60) or X-ray

Manuscript received 22 February 2023; revised 28 February 2023 and 9 March 2023; accepted 18 March 2023. Date of publication 22 March 2023; date of current version 16 August 2023. This work was supported by the European Union's Horizon 2020 Research and Innovation Programme under Grant 101008126.

Rubén García Alía and Matteo Cecchetto are with CERN, 1211 Geneva, Switzerland (e-mail: ruben.garcia.alia@cern.ch).

Andrea Coronetti is with CERN, 1211 Geneva, Switzerland, and also with the Institut d'Électronique et des Systèmes, Université de Montpellier, 34090 Montpellier, France.

Kacper Bilko is with CERN, 1211 Geneva, Switzerland, and also with the Institut d'Optique Graduate School, Laboratoire Hubert Curien UMR 5516, Université de Lyon, 42023 Saint-Etienne, France.

Gerd Datzmann is with Datzmann Interact and Innovate, 80997 Munich, Germany.

Salvatore Fiore is with ENEA Centro Ricerche Frascati, 00044 Frascati, Italy.

Sylvain Girard is with UJM Saint-Etienne, CNRS, Institut d'Optique Graduate School, Laboratoire Hubert Curien UMR 5516, Université de Lyon, 42023 Saint-Étienne, France.

Color versions of one or more figures in this article are available at https://doi.org/10.1109/TNS.2023.3260309.

Digital Object Identifier 10.1109/TNS.2023.3260309

machines, are not. However, as we will later show, part of the research activities in RADNEXT are devoted to cumulative radiation effects in electronics, including comparisons among TID effects induced by different types of radiation fields.

As introduced above, one of RADNEXT's main ambitions is to ease the access to accelerator infrastructure for radiation effects' users and, to do so, the intercomparison across facilities offering similar beams is essential to ensure an independence of the results with regard to the specific facility and beam, hence broadening the access options to fulfill a given radiation testing need. This article in particular deals with the challenge of comparing beams from different heavy ion facilities, having similar LET values but very different energies. In this case, the main purpose is not so much that of enhancing the overall irradiation capability horizontally (i.e., by comparing facilities with similar capabilities), but rather vertically, through the inclusion of high-energy heavy ion beams in the radiation effects' testing offer, which are especially suited for radiation effects' experiments requiring a high penetration capacity (e.g., complex packaging, 3-D structures, board-level testing). Therefore, whereas LET can be regarded as the key figure-of-merit for heavy ion testing, our work investigates the impact of ion energy for comparable LET values, especially in terms of beam fragmentation (analyzed through the event-by-event energy deposition distribution in a solid-state silicon detector) as well as SEUs and MCUs in commercial SRAMs.

After the introduction of RADNEXT and its scientific and technical motivation, this article is structured as follows: the research objectives of RADNEXT are described in Section II. After this, an example of an irradiation campaign targeting a subset of the RADNEXT scientific objectives is described in Section III, focusing on the comparison of radiation–matter interaction and radiation effects among heavy ion beams of similar LET values in very different energy ranges. The conclusions and outlook related to this work are included in Section IV. In addition, logistical details of the RADNEXT project and its transnational beam access workflow are provided in the Appendices.

II. Joint-Research Activities

Joint-research activities within European infrastructure projects have as an objective the improvement, in quality and/or quantity, of the integrated services provided at European level by the infrastructures. Within RADNEXT, there are four work packages (WPs) dedicated to joint-research activities, as given below.

1) WP5: Radiation monitors, dosimeters, and beam characterization.
2) WP6: Standardization of system-level radiation qualification methodology.
3) WP7: Cumulative radiation effects on electronics.
4) WP8: Complementary modeling tools.

WP5 is devoted to the harmonization of dosimetry techniques among different facilities and beams. It is also concerned with the development of innovative instrumentation to improve beam characterization and measurement. This includes optical-fiber dosimetry and use of 3-D NAND Flash single-event upset (SEU)-based monitors and neutron field monitors. One example of this activity was the recent calibration of multimode phosphosilicate optical fibers [2].

WP6 is devoted to defining guidelines for radiation qualification of complex integrated circuits and full mixed digital–analog systems. Building on the RADSAGA experience and outcome on this topic [3], the main focus of this WP is on determining the optimal setup and stimuli to be applied to a complex digital system to qualify its operation under radiation. This already resulted in the publication of a first set of approaches and tools devoted to this objective [4]. Tests were also conducted to investigate the impact of cache memories on the error rate of Linux systems [5] and to the evaluation of reduced resolution redundancy for radiation hardening of systems on chip [6].

WP7 is devoted to the study of cumulative radiation effects, i.e., TID and TNID, with the objective of deepening the knowledge about these effects in the most innovative technologies and proposing test methodologies. One such methodology concerns the use of X-ray generators for TID testing [7] as opposed to the more standard γ-ray sources, e.g., Co-60.

WP8 is devoted to the development and distribution of simulation tools that can reproduce radiation effects in innovative technologies and to the study of nonstandard SEE sensitivities. Concerning the first point, a FLUKA [8], [9] Monte Carlo SEE tool will be developed with the particular focus of enhancing simulations of SEEs induced by low- and intermediate-energy neutrons (<20 MeV), as a follow-up of the work presented in [10]. Moreover, results from this WP have led to a recent publication about an analytical approach to calculate soft error rates induced by atmospheric neutrons, focusing on the 1–10-MeV neutron interval [11].

III. TA Campaign Study Case: Comparing Standard and High-Energy Heavy Ion Beam Results

In addition to the research activities described in the previous section, another critical part of the RADNEXT project is the provision of irradiation beam time in its broad facility network to radiation effects' users worldwide. The related beam provision workflow and the associated key performance indicators of the first 18 months of the project can be found in Appendix C. This section describes an example of an irradiation test campaign performed within the RADNEXT beam access framework and motivated by RADNEXT research objectives.

As introduced above, one of the key objectives of RADNEXT is that of harmonizing irradiation approaches and facilities, as well as providing solutions for emerging irradiation needs. In particular and as outlined in Table I, high-energy heavy ions are of special interest for testing boards and complex components for which the limited range of traditional heavy ion beams poses serious constraints and can even in some cases be a showstopper for testing. However, very few facilities worldwide can provide very high-energy (>100 MeV/n) ions for radiation effects testing and, moreover, such tests are not fully covered by the existing SEE standards.

With this in mind, a RADNEXT TA experimental campaign was proposed in January 2022 and executed in April 2022 by

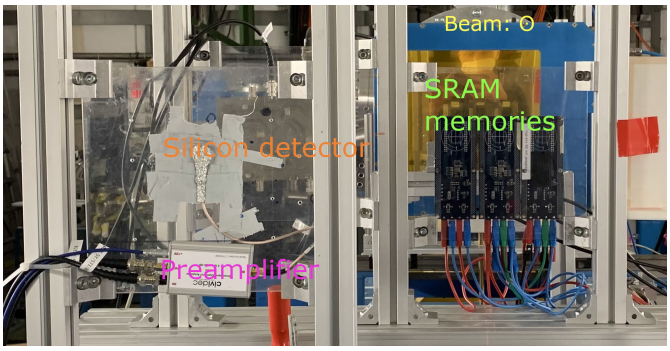

Fig. 1. Experimental setup during the campaign in the GSI SIS-18 facility, containing SRAM memories and the Canberra silicon solid-state detector.

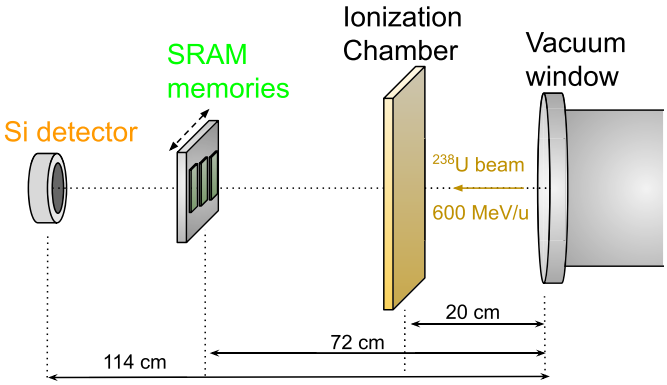

Fig. 2. Schematic drawing of the experimental setup in the GSI SIS-18 facility (dimensions are not preserved). Depending on the DUT, the SRAM memories could be moved outside of the beam.

two of its partners (CERN and GSI) making use of high-energy ion beams available at GSI SIS-18. The main objectives of this proposal were: 1) the intercomparison among different facilities in terms of radiation effects' equivalence and 2) the development of benchmarks required to increase the overall beam time offer while preserving high beam quality in new facilities, such as CHIMERA [12], in development at CERN. Out of the 32 h of beam time requested, 16 were approved, mainly due to the reduced overall beam time offered at GSI throughout RADNEXT. The proposal included irradiation with uranium and iron ions; however, finally only the first could be completed, due to an issue in the ion source. The impact of this unavailability on the overall experiment success was limited, as the priority was clearly on the ^{238}U beam, thanks to its larger LET (rendering it more interesting for radiation effects' applications) and higher resemblance to the lead ions typically used in the CERN accelerator complex.

During this campaign, ^{238}U ions were accelerated by the synchrotron to primary energies of 150–190–330–600–800 MeV/u (corresponding to LETs of 33–29–22–17–15 MeVcm^2/mg, respectively). The test setups used to compare standard ion energy and high ion energy effects were based on a silicon solid-state detector used to collect energy deposition events and a pair of commercial SRAMs. Both the silicon detector and SRAMs had been previously tested in several lower energy heavy ion facilities, also part of the RADNEXT network. The test setups are shown in Fig. 1 as seen from the backside, with a schematic side view depicted in Fig. 2.

Irradiation was performed in air, which simplifies the electrical and mechanical connection constraints with respect to facilities using vacuum chambers. The precise collimation and negligible stray field allow placing the power conditioning and data acquisition units (including laptops) at 2–3 m from the devices under test. These systems are controlled from the control room through a point-to-point ethernet connection. Thanks to this configuration, high-quality signals from the diode can be collected with very little noise.

A. Silicon Solid-State Detector

Silicon solid-state detectors are excellent instruments for characterizing a broad variety of radiation beams and environment properties. Their capability of measuring energy deposition on an event-by-event basis yields valuable information about the absolute particle flux, as well as its composition and how it interacts with matter. Some examples of setups similar or analogous to the one used in this work can be found in [13], [14], and [15].

The irradiation at the standard energy range was performed at RADEF with the 16.3 MeV/u ^{57}Fe heavy ion beam, whereas a high-energy (150–800 MeV/u) heavy ion ^{238}U beam was provided by the GSI SIS-18 facility. The device under test (DUT) was a reverse-biased, fully depleted, 300-μm-thick, silicon solid-state detector manufactured by Canberra (model: FD 50-14-300 RM), with a 0.5 cm^2 directly exposed silicon surface.

The signal was amplified through a CIVIDEC C1-HV current-sensitive preamplifier (21.9 dB of amplification) and attenuated by 6 dB during ^{238}U irradiations to be compliant with the 1-V dynamic range of the CAEN DT5751 1 Gs/s digitizer used to acquire the signal. The diode was connected to the preamplifier using 30-cm RG316 coaxial cable, to comply with the high-frequency signal and ensure low loss before amplification. After the amplifier, the signal was transmitted to the digitizer via 3-m RG58 BNC cable.

The outcome of each energy deposition event is the current as a function of time, later converted into the collected charge. The measured number of charges is converted into deposited energy through the factors obtained during a calibration campaign with standard energy heavy ion beams, outside the scope of this article. Examples of the transients for events caused by the direct ionization from standard energy ^{57}Fe and VHE ^{238}U ions which interact with the sensitive detector silicon area directly are depicted in Fig. 3. As can be (qualitatively) seen, despite the similar amplitude, the signal from the ion depositing the energy in a smaller region (i.e., the ^{57}Fe ion, which stops in the diode-sensitive thickness, and therefore deposits most of its energy in the Bragg peak region) has a slower fall off, due to the impact of plasma screening on charge collection.

The main difference between the two depicted irradiations is the range of the beams in silicon: 1) for the ^{57}Fe, smaller than the thickness of the detector and 2) for the ^{238}U, exceeding 300 μm. The distribution resulting from integrating the

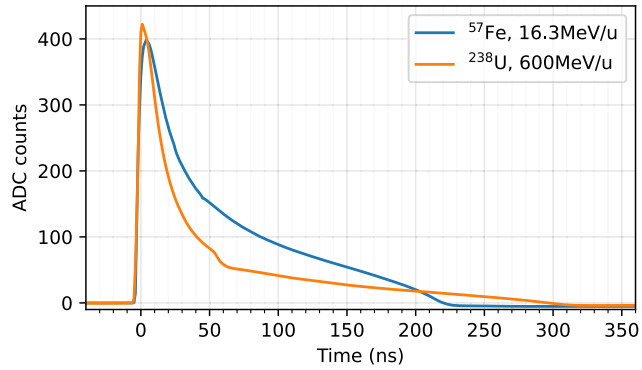

Fig. 3. Measured transients for direct ionization events during ^{57}Fe and ^{238}U irradiations. The traces are baseline subtracted. The energy deposition spectra for the corresponding irradiations are depicted in Fig. 4. Despite the integral of the ^{57}Fe transient being larger than that of the ^{238}U, the energy physically deposited in the diode is larger for the latter, which, however, has an extra 6-dB attenuation in its acquisition.

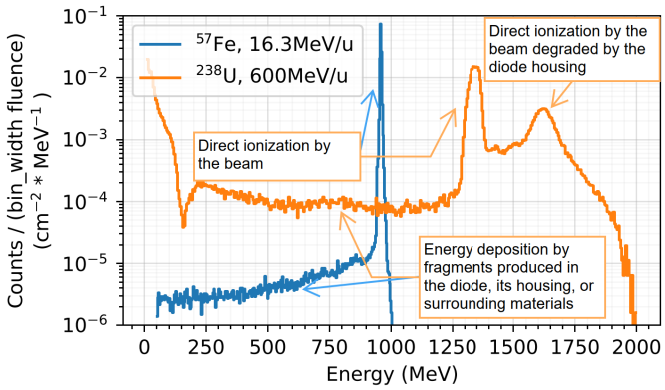

Fig. 4. Energy deposited in the silicon solid-state detectors for irradiations at standard and high-energy heavy ion beams. The 600-MeV/u ^{238}U beam was provided within the scope of the RADNEXT project by the GSI SIS-18.

individual pulses (see Fig. 3) is shown Fig. 4 for the two beams considered. In the case of the standard energy ^{57}Fe beam, the maximum energy deposition spectrum corresponds to the pure direct ionization directly from the heavy ion, leading to the total beam energy corresponding to energy deposition. The tail at lower energies is due to the energy deposition events by the fragments produced either directly in the silicon or in the surrounding elements (beamline or diode casing).

Whereas a thorough and quantitative analysis and benchmark of the nuclear reactions responsible for the off-peak events is beyond the scope of this article, we have used the FLUKA Monte Carlo code to qualitatively assess the nature of these reactions, and how they give rise to a lower amount of deposited energy in the diode when compared with direct ionization peaks. Multiple nuclear reactions between the incident 16.3-MeV/u ^{57}Fe beam and silicon were simulated, one characteristic example of which is described as follows:

$$^{57}\mathrm{Fe} + ^{28}\mathrm{Si} \rightarrow ^{78}\mathrm{Kr} + ^{2}\mathrm{H} + 3p + n.$$

In this reaction, a 8.4−MeV/u krypton fusion compound is produced, with a significantly larger mass (Z = 78) and LET (33.4 MeVcm^2/mg, versus 13.5 MeVcm^2/mg of the incident ^{57}Fe beam) than the original projectile and target nucleus. The impact of these high-LET ion-nucleus reaction products on the so-called sub-LET threshold SEE cross section is discussed in [16] and [17]. This fusion product is relatively short-ranged (80 μm) and will therefore typically deposit its full energy within the active volume of the sensor. In addition, light fragments (a deuterium, a neutron, and three protons) are also produced, with energies between 5 and 80 MeV, and having in most cases ranges significantly larger than the diode dimensions. Therefore, a fraction of the initial ion energy is lost, first, because the sum of the energies of the reaction products (855 MeV) is smaller than the projectile total kinetic energy (929 MeV) due to the energy lost in the nuclear reaction. And second, because a large fraction of the energy transferred to the light fragments is not deposited within the diode's sensitive volume.

In the case of the ^{238}U beam, provided through the RADNEXT project, the peak corresponding to the direct ionization is at ∼1.3 GeV, which is consistent with the LET value of the projectile (17 MeVcm^2/mg) equal, when considering the silicon density, to 4.0 GeV/cm). In addition, at ∼1.6 GeV, there is a second peak corresponding to direct ionization of the beam that loses energy in the diode casing, as the active region is partially shielded, and results in a higher LET value and, in turn, larger deposited energy [18], [19].

Moreover, as can be seen, the relative fragmentation (i.e., off-peak) level is significantly larger for the high-energy heavy ion beam, when compared with the standard energy one. Also, the type of nuclear reaction taking place at this much larger energy regime is also very different to the one shown above. As an example, the following characteristic nuclear reaction is considered:

$$^{238}\mathrm{U} + ^{28}\mathrm{Si} \rightarrow ^{123}\mathrm{Xe} + ^{9}\mathrm{Be} + 8\alpha + 50H + 30n$$

in which, along with the forwardly directed projectile-like product, xenon-123 (with an energy of 585 MeV/u, similar to the incident ion) a plethora of light particles are produced, including a 690 − MeV/u beryllium-9 ion, eight helium isotopes, with a maximum (total) energy of 2.9 GeV, 50 hydrogen isotopes (mainly protons) of maximum energy 2.1 GeV, and 30 neutrons, with a maximum energy of 775 MeV. Therefore, as a result of the reaction, a projectile of similar energy per nucleon, but lower mass (and hence LET), is produced, along with multiple energetic light fragments, which only deposit a small fraction of their energy in the diode, hence also leading to lower energy deposition values than the primary peak, corresponding to direct ionization losses of ions that do not interact via nuclear reaction.

In summary and from a perspective of the dominant (in terms of mass) reaction product, heavy ion nuclear interactions at standard SEE testing energies (10–20 MeV/n) will create a massive (with respect to the projectile and target), high-LET low-ranged recoil, whereas reaction products at hundreds of MeV/u will have lighter masses than the original projectile, but will preserve its energy per nucleon and therefore also be very long-ranged.

Moreover, by integrating the number of primary energy deposition peak counts and dividing them by the diode sensitive surface and time, the instrument can be used to measure the instantaneous beam flux as a function of time, as shown

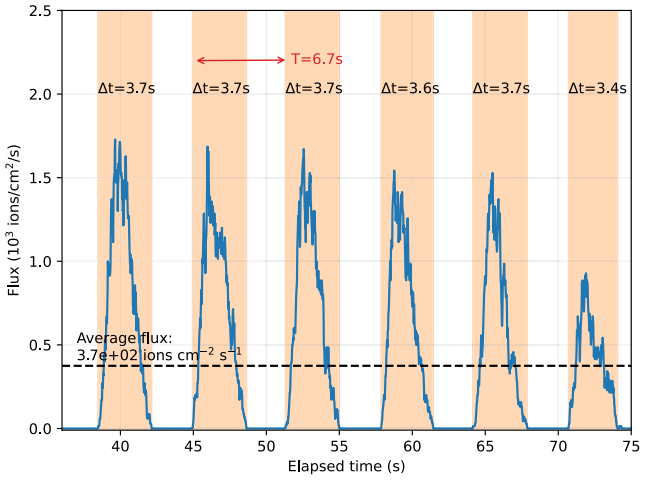

Fig. 5. Example of how the solid-state silicon detector is used to measure the instantaneous flux of the GSI beam, in this case for 150-MeV/u ^{238}U ions.

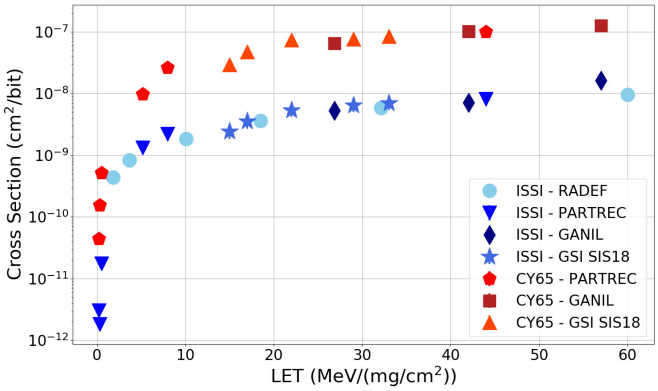

Fig. 6. Heavy ion SEU cross sections of two commercial SRAMs as a function of LET to compare the measurements obtained with ions of different energies (16.3-MeV/u RADEF, 10–90-MeV/u PARTREC, 10–50-MeV/u GANIL, and 150–800-MeV/u GSI SIS-18).

in Fig. 5, illustrating also the spill structure of the GSI heavy ion synchrotron.

B. SRAMs

The two SRAMs considered in this study are the IS61WV204816BLL-10TLI (40 nm, 32 Mbits, datecode 1650) and the CY62167GE30-45ZXI (65 nm, 16 Mbits, datecode 1731). The test procedure and the data for other ion beams (RADEF [20], PARTREC [21] and GANIL [22]) are available from a previous publication [23].

Similar test procedures were followed for this test at GSI. The SRAMs were biased at 3.3 V I/O, and they were written with a checkerboard pattern and were read periodically during irradiation (each 2 s) correcting the bits that were found in error. Both the devices were delidded, as it was the case for previous heavy ion irradiations elsewhere.

A first comparison between standard and high ion energies can be achieved by contrasting the SEU cross sections measured at various facilities. This is available in Fig. 6, where the SEU cross sections of the two SRAMs are plotted as a function of LET of the primary ions.

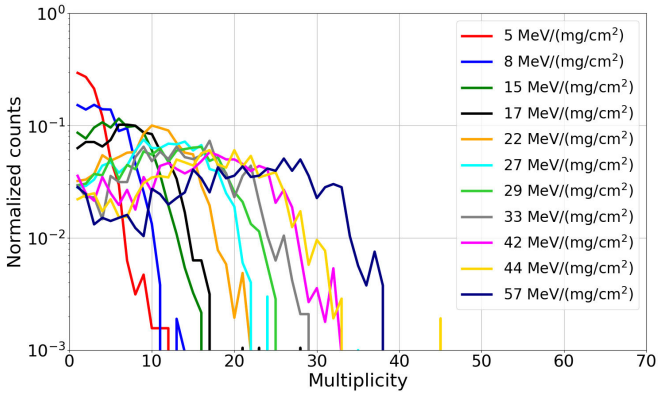

Fig. 7. Probability distributions of multiplicities of MCUs as a function of the ion LET to compare with the measurements obtained with ions of different energies, but similar LET [5-, 8-, 44-MeV/(mg/cm^2) PARTREC, 27-, 42-, 57-MeV/(mg/cm^2) GANIL, and 15-, 17-, 22-, 29-, 33-MeV/(mg/cm^2) GSI SIS-18].

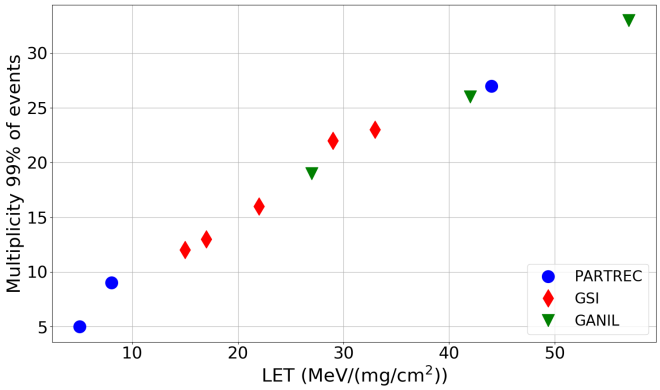

Fig. 8. Same data as plotted in Fig. 7 but extracting a single MCU multiplicity value (in this case, the 99 percentile) per LET point, and again showing the independence of the MCU multiplicity on the beam energy (and, therefore, facility) for a given LET value.

The cross sections were measured on a single device at each facility. The data are reported with error bars with 95% confidence level based on a 10% uncertainty on the measured fluence at each facility. If not visible, they are smaller than the marker. We note that for the RADEF, PARTREC, and GANIL data, the fluence for the cross section calculation was that given by the facility dosimetry systems. For GSI, the fluence was determined from the diode measurements introduced in the previous section.

For the LET interval of consideration during the GSI SIS-18 tests, for both the SRAMs, the cross sections are already approaching saturation. However, it can be concluded that the cross sections measured with high-energy ions are well-aligned with respect to the data points for nearby LETs measured with standard energy ions.

For the CY62167GE30-45ZXI, it was also possible to perform a multiple-cell upset (MCU) data analysis by means of the algorithms presented by LIRMM [24], [25]. The purpose of this analysis is to verify whether high-energy ions would induce MCUs with different characteristics with respect to standard energy ions, typically due to high-energy δ rays

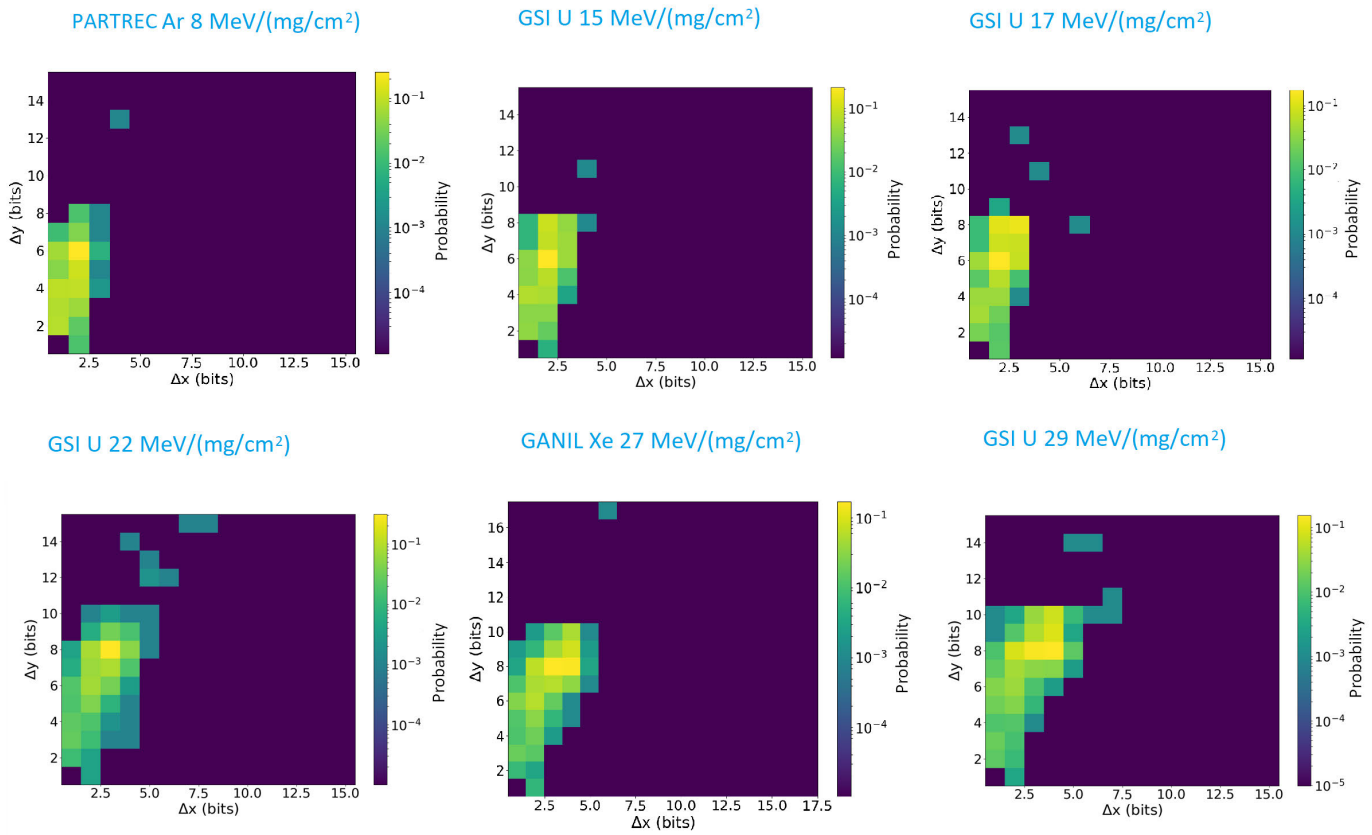

Fig. 9. Heatmaps classifying the probability of an MCU having a certain shape in the bit-line (x) or word-line (y) to compare with the measurements obtained with ions of different energies, but similar LET [8-MeV/(mg/cm^2) PARTREC, 27-MeV/(mg/cm^2) GANIL, and 15-, 17-, 22-, 29-MeV/(mg/cm^2) GSI SIS-18].

produced by the high-energy ions, as was shown in the past [26].

Fig. 7 portrays a histogram of the probability distributions of the multiplicity of the MCU clusters for ions with various LETs. It can be noted that the distributions have a flat-top shape that falls down very fast. This result differs from some previous observations [27], where Gaussian distributions of the multiplicity as a function of LET were reported. As the LET of the ion increases, the flat top enlarges and the maximum multiplicity moves toward higher values.

When comparing the GSI distribution functions [15, 17, 22, 29, 33 MeV/(mg/cm^2)] with those of other ions of similar LET, but lower energy, it can be noted that there are no significant differences and that the GSI distributions fall in between those of the other facilities. For instance, the 27-MeV/(mg/cm^2) from GANIL and the 29-MeV/(mg/cm^2) from GSI have very similar flat tops and the first falls off at a slightly lower multiplicity than the second.

The correlation between the MCU multiplicity and LET can better be observed in Fig. 8, showing that the dependence of the multiplicity with the LET is independent of the ion energy, and hence on the facility where the data are collected. Such a correlation also shows the potential of this MCU detection solution (and its related calibration) to retrieve the LET value of ion beams.

An additional analysis to compare the MCU is reported in Fig. 9. The heatmaps (i.e., with different pixel colors representing different probabilities, as per the code to the right of each plot) report the probability that an MCU would have a certain extension among adjacent bit-lines (x) and among adjacent word-lines (y). For instance, for the 8-MeV/(mg/cm^2) plot, only MCUs having a maximum extension over three bit-lines and eight word-lines are seen (except for one outlier) and the maximum likelihood for an ion of this LET is to generate an MCU with a shape extending for two bit-lines and six word-lines.

As the heatmaps show, the MCU shapes change when the LET is increased. In a similar fashion as for the multiplicity, the MCUs involve a growing number of bit-lines and word-lines. Note that the distributions at 8 and 15 MeV/(mg/cm^2) are very similar, both in terms of maximum extension along bit-line and word-line as well as the maximum likelihood. Something similar can be said for the 27- and 29-MeV/(mg/cm^2) cases. In addition, the 17-MeV/(mg/cm^2) case seems to have double maxima that correspond to those of 15 and 22 MeV/(mg/cm^2), respectively.

Letting aside the very few outliers appearing in all the plots, one can conclude that the MCU dimensions and maximum likelihood for certain shapes seem to be independent of the ion energy and only correlated with the ion LET. Therefore, the MCU analysis seems to point out that no apparent difference exists between standard energy and high-energy ions for what concerns the generation of clusters of bits in error for this technology and component.

IV. Conclusion

Throughout its first 18 months of existence, RADNEXT has succeeded in implementing an efficient TA scheme providing EU-funded beam time for worldwide radiation effects' users across a very broad range of facilities, covering a large irradiation parameter phase space and including an important level of redundancy for the beam types in highest demand by the user community.

As shown in this article, the beam access and research activities developed within RADNEXT are already contributing to increase the diversity and harmonization levels across European facilities. Moreover, the RADNEXT transnational beam access activities are complemented by a research program oriented at improving the radiation effects' testing life cycle, and including notably facility benchmarks to increase the overall network robustness and capacity. An example of such an intercomparison is shown for two heavy ion facilities, covering a similar LET interval, but in very different energy regimes, and highlighting both the similarities (compatible SEU and MCU cross sections for 65-nm technology commercial SRAMs) and differences (nuclear reaction characteristics) among them.

More specifically, the solid-state detector energy distribution measurements show that as expected and supported by the Monte Carlo simulations, the presence of nuclear fragments in high-energy heavy ion beams is significantly stronger than the one in standard energy beams. Therefore, the possible impact of such fragments on the experimental results needs to be carefully assessed. However, as demonstrated by the very satisfactory SEU cross section agreement across the different energy regimes, the fragment impact on this particular experiment can be considered negligible. In addition to its fragmentation detection capabilities, the solid-state detector is also validated as a reliable means of determining the beam flux with a time resolution that comfortably allows for the measurement of the evolution of the flux within the ∼3.7-s beam spill at GSI.

Moreover, as shown in the detailed MCU analysis presented in this article, the differences in the ionization track structures for the different ion energies do not have an impact on the MCU probability and multiplicity which, whereas depending strongly on the LET, is experimentally shown to be independent of energy in the interval studied in this work.

Given the rapidly developing interest of the radiation effects' community in using VHE ion beams for radiation effects testing, we expect such beam characterization and intercomparison studies to play an important role in the near future, contributing to develop best practice recommendations and guidelines when using such beams, not only at the SIS-18 facility in GSI covered in this work but also in other VHE ion infrastructures such as NSRL in BNL or CHIMERA at CERN.

Appendix A
RADNEXT Partners and Structure

The RADNEXT project consists of 31 beneficiaries (full list available on the RADNEXT website [1]), 19 of which offer transnational beam access to one or multiple facilities, as presented in Table II. These beneficiaries, along with the nine partners, are also involved in the project, through a WP structure that includes management (WP1), networking (WP2–WP4), and research (WP5–WP8) activities, with WP3 being devoted to the transnational beam access coordination, and WPs 9 and 10 to the beam access provision for atmospheric and space environment applications, respectively.

Appendix B
RADNEXT Service-Related Motivation

The RADNEXT network is aimed at mitigating some of the key barriers for accelerator infrastructure access to radiation effects' testing users. These barriers, as carefully analyzed during the RADNEXT proposal preparation, are often linked to the limited availability of the accelerator infrastructure for irradiation purposes, which can in turn derive from: infrastructure priority for fundamental research or medical applications; temporary shutdown for maintenance or upgrades; and permanent shutdown due to lack of funding from main funding bodies, all of which typically result in long lead scheduling procedures, often not compatible with the user needs and related project timelines.

In addition to the limited facility availability, both in absolute terms and relative to the increasing irradiation demand, the user technical and administrative support (i.e., the provision of a professional service to users, including notably industry) can also be a significant entry barrier for facilities interested in offering beam for irradiation applications, as well as for users interested in accessing it.

Moreover, the cost of the beam time is also an important factor for users. However, according to a study based on a large amount of interviews to radiation effects' users carried out in preparation of the RADNEXT proposal, this factor is less important than others already introduced, such as the technical compliance in terms of beam type and properties, the availability and ease of access to the facility, and the quality and customer orientation of the related services. And, it is worth recalling that as shown and discussed in [28], the cost of beam time is far from dominant when considering the overall costs of the tests, mainly driven by qualified radiation effects' workforce during the preparatory phases of the test.

Related to the points above, RADNEXT's ambition is that of acting as an enabler for radiation effects testing in accelerator and reactor infrastructure, being a relevant driver in terms of technology transfer and innovation for Europe's high-tech industry, namely, by:

1) providing a professional service to users (i.e., mindset for customer focus), notably valuing reliability and responsiveness;
2) explicitly supporting the involvement of project partners in technology transfer activities;
3) enhancing the visibility and awareness of facilities, and bridging the gap between different working cultures in academia and research laboratories (usually running the facilities) and industry (usual users);
4) diversifying the type of facilities available for radiation effects' testing, and generating redundancy for beam

TABLE I
KEY SEE TESTING REQUIREMENTS FOR VARIOUS RADIATION ENVIRONMENTS AND APPLICATIONS

Environment and application	Key SEE testing requirements
Space: according to standards [29]	• Mainly heavy ions, with the requirement of reaching high LET values (∼60-80 MeVcm^2/mg); • Focus on component level testing of "space grade" and/or "rad-hard" parts which, for high LET testing, typically require part de-lidding and testing in vacuum; • Proton SEE testing may be required as well (see below), however in some cases the related sensitivity and rates can be estimated based on heavy-ion response [30];
Space: emerging needs [31]	• Increasing interest in Commercial Off-The-Shelf (COTS) components; • More relaxed maximum LET requirements for heavy ions (e.g., 40 MeVcm^2/mg, just above the iron knee [32]) with protons (i.e., indirect energy deposition up to ∼ 15 MeVcm^2/mg) sometimes being sufficient • ∼200 MeV-requirement for proton testing, to cover a large fraction of the trapped proton spectrum, and provide large enough secondary LET if used as heavy-ion proxy [33], [34] (linked to point above); • Fluxes up to ∼10^8 p/cm^2/s for component level, in order to reach fluences of ∼10^{10} – 10^{11} p/cm^2. Board/system level tests will typically require lower fluxes and fluences, also in view of minimizing cumulative damage; • Strong interest in board and system level testing, as well as complex packages, therefore the beam/field size and penetration is often prioritized versus the maximum LET [35]; • Possible impact of low energy protons on in-orbit SEE rate [36], [37];
High-reliability atmospheric applications [38]	• Mainly focused on COTS components, modules and systems; • Spallation neutrons generating an atmospheric-like spectrum, and/or (quasi) monoenergetic neutrons or protons, reaching energies up to a few hundred MeV; • Fluxes up to 10^6 particles/cm^2/s typically provide sufficient acceleration factors. Roughly two orders of magnitude lower fluxes for system level testing; • Strong interest in board- and system-level testing; • Cumulative effects are not relevant, therefore test conditions are tailored to exclude them;
High-energy accelerators [39]	• Mainly focused on COTS components for custom designs; • Similar to high-reliability atmospheric applications (see above), with the following main differences: – component level testing fluxes typically need to reach ∼10^8 p/cm^2/s – in some cases, combined SEE/cumulative damage is desirable – System level tests performed in mixed-field facilities [40], in order to account for both stochastic and cumulative damage • Other applications that would have a large overlap with this application: – Electronics for high-energy accelerator detectors, with the main differences of (i) being mainly focused on rad-hard designs and (ii) requiring larger fluences, and/or heavy-ion SEE data, to convert to proton, neutron and pion (i.e., hadron) SEE rates; – Electronics for medical accelerators, mainly interested in neutrons up to a maximum energy of around 20 MeV for conventional radiotherapy, and ∼200 MeV for proton therapy; – Electronics for fusion applications [41], mainly interested in neutrons up to a maximum energy of 14 MeV;

types in high demand, hence mitigating the risk associated with the reduction or even full interruption of beam provision by a given facility; and

TABLE II
HIGH-LEVEL BEAM AND FACILITY ACCESSES PROVIDED THROUGH RADNEXT TA

Facility	Beam Type	Energy (MeV/n)	Flux (pp/cm^2/s)	Beam time available (h)
TRIUMF BL1B (CA)	Protons	360-480	10^2-10^9	120
PSI (CH)	Protons	6-230	10^2-10^9	130
NPI-CAS (CZ)	Protons	6-35	10^9-10^{12}	40
HZDR DRACO (DE)	Protons	80-250	O(10^{10})	120
CLPU (ES)	Protons	spectrum	O(10^{10}	150
CNA (ES)	Protons	0.5-18	10^3-10^{12}	200
RADEF (FI)	Protons	0.5-55	10^2-10^8	45
PARTREC (NL)	Protons	30-190	10^2-10^8	238
Protons				1043
CHARM (CH)	Ions	6000	10^5-10^6	500
UCL (BE)	Ions	9.3	10^1-10^4	280
GSI SIS18 (DE)	Ions	80-2000	10^2-10^8	64
GSI UNILAC (DE)	Ions	3.4-11.4	10^0-10^{10}	128
RADEF (FI)	Ions	9.3-22	10^2-10^5	255
GANIL (FR)	Ions	4-95	10^1-10^4	158
PARTREC (NL)	Ions	30-90	10^2-10^8	237
Ions				1622
CHARM (CH)	Mixed-field	spectrum	O(10^6)	800
TRIUMF TNF (CA)	Neutrons	spectrum	O(10^6)	92
CHIPIR (UK)	Neutrons	spectrum	O(10^6)	620
Neutrons atmospheric				712
NPI-CAS (CZ)	Neutrons	spectrum	10^7-10^{10}	40
GANIL NFS (FR)	Neutrons	spectrum		90
HZDR nELBE (DE)	Neutrons	spectrum	O(10^7)	150
Neutrons spectrum				280
PTB (DE)	Neutrons	0.144-17	O(10^7)	175
LPSC (FR)	Neutrons	2.5-14	O(10^7)	160
FNG (IT)	Neutrons	2.5-14	O(10^8)	530
NESSA (SE)	Neutrons	14		100
Neutrons mono-energetic				965
ILL (FR)	Neutrons	2.5 × 10^{-11}	O(10^9)	100
EMMA (UK)	Neutrons	2.5 × 10^{-11}	O(10^6)	150
Neutrons thermal				250
RIKEN-RAL (UK)	Muons	1-60		140
HZDR eLEBE (DE)	Electrons	spectrum	O(10^7)	80
HZDR gELBE (DE)	γ-rays	spectrum	O(10^7)	80
ESRF (FR)	X-rays	0.02	O(10^{11})	288
Total				6260

5) acting as a source of stable revenue, which can at least partially satisfy the need of financial support for running the accelerators.

APPENDIX C
RADNEXT TRANSNATIONAL FACILITY ACCESS: WORKFLOW AND STATISTICS

The RADNEXT TA workflow is presented in Fig. 10 and can be summarized as follows:

1) The TA call for proposals is open for 30 days. During this period, users can send their proposals to the RADNEXT network through a dedicated online portal (radnext-ta-portal.web.cern.ch). The proposals are lightweight, though still divided into three parts: excellence, impact, and implementation with a character count limit set to 4500 for the whole proposal. These calls for proposals reopen quarterly during the year and are open to users worldwide, with a quota for countries not pertaining to the Horizon 2020 EU program of up to 20%. A proposal is not directly linked to a facility, but rather to a beam type. If a user needs to test a given part (or set of parts) in different beam types, multiple proposals are required.

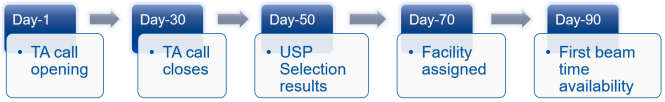

Fig. 10. TA workflow for proposals submitted to RADNEXT.

2) All the proposals are assigned for evaluation to a USP, which is composed of TA WP leaders and members of the industrial and scientific advisory panels. Overall, at least 50% of the USP reviewers are external to the RADNEXT project. The USP provides feedback in the form of an evaluation of excellence, impact, and implementation of each proposal and comments. Then, the highest scoring proposals are awarded RADNEXT TA beam time.
3) Accepted proposals are then assigned to a facility within the network that satisfies the requirements for the test mentioned by the user in the proposal. The user is put in contact with the facility coordinator for technical discussion and to schedule the test.
4) Depending on the facility availability and the user setup readiness, the beam time can be awarded as early as two months after the call closure and as late as nine months. Users accessing beam through RADNEXT are committed to publishing their irradiation results, for which a first summary version of the user report can be found in the RADNEXT Zenodo community [42].

Regarding the publication obligation, RADNEXT is well aware that this can be an entry barrier for companies performing tests involving proprietary and strategic information and results. Therefore, the consortium is considering a "second path" to be possibly offered to users in the future, which would consist in paid access, hence not subject to publication obligation, but still benefiting from the advantages provided by RADNEXT in terms of the centralized access point and optimized facility assignment.

Throughout the first six calls for beam time (1.5 years), RADNEXT TA received 148 proposals, out of which 86 were accepted (58% acceptance rate). All the proposals at this stage have been assigned a facility, having resulted in the completion of 41 tests, with the remainder of the tests to be accomplished in 2023. Currently, the amount of beam time assigned to facilities has reached 2600 h and the total number of tests executed amounts to more than 1300 h. Out of the 148 received proposals, 46 (i.e., roughly one-third) come from industry.

As to what concerns rejected proposals still falling in the RADNEXT scope, they are encouraged to resubmit and are provided both with reviewer feedback on how to improve their proposal and with the option of receiving further support from the RADNEXT user support expert (USE) team. The USE consists of experienced radiation effects experts from academia and industry who offer assistance to less experienced users in the process of drafting TA proposals, advising on project-specific aspects to avoid unrealistic planning, identifying, and mitigating potential risks, and integrating the expert's experience into the test plans.

In relation to the paragraph above, it is worth highlighting that out of the 22 resubmitted proposals RADNEXT received, 15 (68%) were accepted, hence clearly showing the improvement in the proposal quality and related acceptance rate.

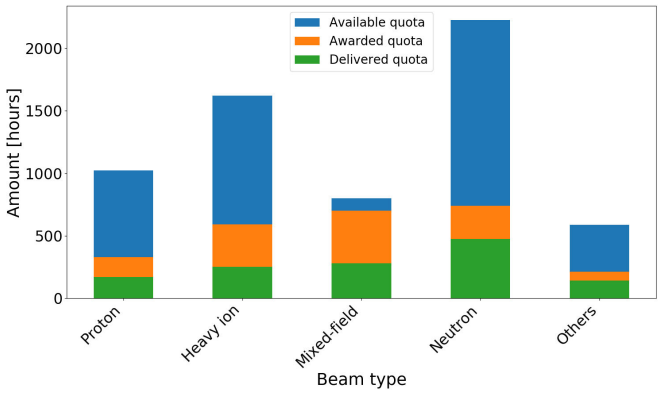

Fig. 11. Histogram reporting the current progression in terms of hours assigned and already delivered to users with respect to total availability for each beam type.

Fig. 11 depicts the overall beam time available in RADNEXT by beam type and how much of it has already been delivered (i.e., with users having completed their tests) or awarded (for users whose tests are scheduled in the coming months). As can be seen, 60% of the beam time for proton, heavy ion, and neutron irradiations is still to be awarded, and there are therefore plenty of opportunities until fall 2024 for users wishing to apply to RADNEXT TA. So far, 32% of the received proposals came from industry, 35% from academia, 28% from research institutes, and 5% from agencies.

The type of tests that have been awarded beam time span a wide variety of objectives, including: 1) the characterization of novel beamlines and irradiation techniques; 2) the exploration of radiation effects in commercial discrete devices, complex integrated circuits and systems; 3) the reliability of artificial intelligence architectures; and 4) the calibration and development of detectors.

Out of the RADNEXT test campaigns already executed, the median time between proposal submission and test completion has been of 190 days, with a 25 (75) percentile of 140 (225) days. The RADNEXT project strives to provide beam time to users with reasonable lead times, which in turn depend mainly on: 1) the duration of the RADNEXT proposal review and facility assignment; 2) the availability of the facilities; and 3) the readiness of the users.

Some of the results obtained by RADNEXT TA users have already been presented at international conferences dedicated to radiation effects in electronics. Among them, some noteworthy examples are the methodology based on fragmented heavy ion beams for electronic testing [43], the single-event upset and multiple-bit upset sensitivity of Flash memories [44], the calibration of CMOS image sensors to be used on nanosatellites [45], and the evaluation of mitigation techniques in the RISC-V processor architectures [46].

ACKNOWLEDGMENT

The authors thank all the members of the RADNEXT project (WP leaders, facility coordinators, doctoral and postdoctoral students, etc.) and its scientific and industrial advisory panels.

REFERENCES

[1] *RADiation Facility Network for the Exploration of Effects for Industry and Research*. Accessed: Jun. 14, 2022. [Online]. Available: https://radnext.web.cern.ch/

[2] L. Weninger et al., "Calibration in the visible and infrared domains of multimode phosphosilicate optical fibers for dosimetry applications," presented at the RADECS, Venice, Italy, Oct. 2022.

[3] A. Coronetti et al., "Radiation hardness assurance through system-level testing: Risk acceptance, facility requirements, test methodology, and data exploitation," *IEEE Trans. Nucl. Sci.*, vol. 68, no. 5, pp. 958–969, May 2021.

[4] L. Matana Luza et al., "Impact of atmospheric and space radiation on sensitive electronic devices," in *Proc. ETS Conf.*, Barcelona, Spain, May 2022, pp. 122–131.

[5] M. Jaksch et al., "Debugging Xilinx Zynq-7000 SoC processor caches during Linux system execution under proton irradiation," in *Proc. IEEE Radiat. Effect Data Workshop*, Provo, UT, USA, Jul. 2022, pp. 105–108.

[6] L. G. Astudillo et al., "Evaluating reduced resolution redundancy for radiation hardening," presented at the RADECS, Venice, Italy, Sep. 2022.

[7] V. Girones et al., "The use of high energy X-ray generators for TID testing of electronic devices," presented at the RADECS, Venice, Italy, Sep. 2022.

[8] G. Battistoni et al., "Overview of the FLUKA code," *Ann. Nucl. Energy*, vol. 82, pp. 10–18, Aug. 2015.

[9] C. Ahdida et al., "New capabilities of the FLUKA multi-purpose code," *Frontiers Phys.*, vol. 9, Jan. 2022, Art. no. 788253.

[10] M. Cecchetto et al., "0.1–10 MeV neutron soft error rate in accelerator and atmospheric environments," *IEEE Trans. Nucl. Sci.*, vol. 68, no. 5, pp. 873–883, May 2021.

[11] F. Wrobel et al., "An analytical approach to calculate soft error rate induced by atmospheric neutrons," *Electronics*, vol. 12, no. 1, p. 104, Jan. 2023.

[12] M. Fraser et al., "Feasibility of slow-extracted high-energy ions from the CERN proton synchrotron for CHARM," in *Proc. 13th Int. Particle Accelerator Conf. (IPAC)*. Bangkok, Thailand, Jun. 2022, pp. 1703–1706.

[13] V. Ferlet-Cavrois et al., "Influence of beam conditions and energy for SEE testing," *IEEE Trans. Nucl. Sci.*, vol. 59, no. 4, pp. 1149–1160, Aug. 2012.

[14] C. Cazzaniga et al., "Measurements of low-energy protons using a silicon detector for application to SEE testing," *IEEE Trans. Nucl. Sci.*, vol. 69, no. 3, pp. 485–490, Mar. 2022.

[15] D. Lucsányi et al., "G4SEE: A Geant4-based single event effect simulation toolkit and its validation through monoenergetic neutron measurements," *IEEE Trans. Nucl. Sci.*, vol. 69, no. 3, pp. 273–281, Mar. 2022.

[16] R. G. Alía et al., "Proton dominance of sub-LET threshold GCR SEE rate," *IEEE Trans. Nucl. Sci.*, vol. 64, no. 1, pp. 388–397, Jan. 2017.

[17] V. Wyrwoll et al., "Heavy ion nuclear reaction impact on SEE testing: From standard to ultra-high energies," *IEEE Trans. Nucl. Sci.*, vol. 67, no. 7, pp. 1590–1598, Jul. 2020.

[18] V. Wyrwoll et al., "Longitudinal direct ionization impact of heavy ions on SEE testing for ultrahigh energies," *IEEE Trans. Nucl. Sci.*, vol. 67, no. 7, pp. 1530–1539, Jul. 2020.

[19] M. Bagatin et al., "Characterizing high-energy ion beams with PIPS detectors," *IEEE Trans. Nucl. Sci.*, vol. 67, no. 7, pp. 1421–1427, Jul. 2019.

[20] A. Virtanen, R. Harboe-Sorensen, A. Javanainen, H. Kettunen, H. Koivisto, and I. Riihimaki, "Upgrades for the RADEF facility," in *Proc. IEEE Radiation Effects Data Workshop*, Jul. 2007, pp. 38–41.

[21] E. R. van der Graaf, R. W. Ostendorf, M. J. van Goethem, H. H. Kiewiet, M. A. Hofstee, and S. Brandenburg, "AGORFIRM, the AGOR facility for irradiations of material," in *Proc. Eur. Conf. Radiat. Effects Compon. Syst.*, Bruges, Belgium, Sep. 2009, pp. 451–454.

[22] M. Moscatello et al., "Industrial applications with GANIL SPIRAL2 facility," in *Proc. RADECS Conf.*, Bremen, Germany, Sep. 2016, pp. 313–315.

[23] A. Coronetti et al., "SEU characterization of commercial and custom-designed SRAMs based on 90-nm technology and below," in *Proc. IEEE Radiat. Effects Data Workshop*, Santa Fe, NM, USA, Dec. 2020, pp. 54–63.

[24] G. Tsiligiannis et al., "Multiple cell upset classification in commercial SRAMs," *IEEE Trans. Nucl. Sci.*, vol. 61, no. 4, pp. 1747–1754, Aug. 2014.

[25] A. Bosser et al., "Investigation on MCU clustering methodologies for cross-section estimation of RAMs," *IEEE Trans. Nucl. Sci.*, vol. 62, no. 6, pp. 2620–2626, Dec. 2015.

[26] M. P. King et al., "The impact of delta-rays on single-event upsets in highly scaled SOI SRAMs," *IEEE Trans. Nucl. Sci.*, vol. 57, no. 6, pp. 3169–3175, Dec. 2010.

[27] G. I. Zebrev and K. S. Zemtsov, "Multiple cell upset cross-section modeling: A possible interpretation for the role of the ion energy-loss straggling and Auger recombination," *Nucl. Instrum. Methods Phys. Res. A, Accel. Spectrom. Detect. Assoc. Equip.*, vol. 827, pp. 1–7, Aug. 2016.

[28] *National Academies of Sciences, Engineering, and Medicine and Others, Testing at the Speed of Light: The State of US Electronic Parts Space Radiation Testing Infrastructure*, National Academies Press, Washington, 2018.

[29] *Single Event Effects Test Method and Guidelines*, Standard ESCC 25100, ESCC-Standard, October, 2014.

[30] C. Weulersse et al., "A Monte-Carlo engineer tool for the prediction of SEU proton cross section from heavy ion data," in *Proc. RADECS Conf.*, Sep. 2011, pp. 376–383.

[31] *Guidelines for the Utilization of COTS Components and Modules in Space*, document ESA-TEC-TN-021473, ESA-Technical-Note, May 2021.

[32] F. Bezerra et al., "Proposal of a lightened radiation hardness assurance methodology for new space," in *Proc. RADECS Conf.*, Vienna, Austria, Sep. 2021, pp. 210–215.

[33] R. Ladbury, J.-M. Lauenstein, and K. P. Hayes, "Use of proton SEE data as a proxy for bounding heavy-ion SEE susceptibility," *IEEE Trans. Nucl. Sci.*, vol. 62, no. 6, pp. 2505–2510, Dec. 2015.

[34] R. G. Alía et al., "Simplified SEE sensitivity screening for COTS components in space," *IEEE Trans. Nucl. Sci.*, vol. 64, no. 2, pp. 882–890, Feb. 2017.

[35] A. deBibikoff and P. Lamberbourg, "Method for system-level testing of COTS electronic board under high-energy heavy ions," *IEEE Trans. Nucl. Sci.*, vol. 67, no. 10, pp. 2179–2187, Oct. 2020.

[36] N. A. Dodds et al., "Hardness assurance for proton direct ionization-induced SEEs using a high-energy proton beam," *IEEE Trans. Nucl. Sci.*, vol. 61, no. 6, pp. 2904–2914, Dec. 2014.

[37] A. Coronetti et al., "Assessment of proton direct ionization for the radiation hardness assurance of deep submicron SRAMs used in space applications," *IEEE Trans. Nucl. Sci.*, vol. 68, no. 5, pp. 937–948, May 2021.

[38] *Measurement and Reporting of Alpha Particle and Terrestrial Cosmic Ray-Induced Soft Errors in Semiconductor Devices*, document JESD89A, JEDEC-Standard, Jan. 2012.

[39] R. Garcia-Alia et al., "Single event effects in high-energy accelerators," *Semicond. Sci. Technol.*, vol. 32, no. 3, Feb. 2017, Art. no. 034003.

[40] D. Prelipcean et al., "Benchmark between measured and simulated radiation level data at the mixed-field CHARM facility at CERN," *IEEE Trans. Nucl. Sci.*, vol. 69, no. 7, pp. 1557–1564, Jul. 2022.

[41] J. L. Autran et al., "Real-time characterization of neutron-induced SEUs in fusion experiments at WEST Tokamak during D-D plasma operation," *IEEE Trans. Nucl. Sci.*, vol. 69, no. 3, pp. 501–511, Mar. 2022.

[42] *RADNEXT Zenodo Community*. Accessed: Jun. 17, 2022. [Online]. Available: https://zenodo.org/communities/radnext/

[43] R. Garcia-Alia et al., "Fragmented high-energy heavy ion beams for electronic testing," *IEEE Trans. Nucl. Sci.*, early access, Oct. 5, 2022, doi: 10.1109/TNS.2022.3210403.

[44] L. Coic et al., "Heavy ion induced SEU and MBU sensitivity of 3D NAND flash structures," presented at the RADECS, Venice, Italy, Oct. 2022.

[45] J. Florczak et al., "Calibration of the deposited energy in CMOS imagers for particle detection on nanosatellites," presented at the RADECS, Venice, Italy, Oct. 2022.

[46] A. Oliveria and F. Kastensmidt, "Evaluating fault tolerant techniques on COTS RISC-V NOEL-V processor in Zynq UltraScale+ FPGA under proton test," presented at the RADECS, Venice, Italy, Oct. 2022.